Proceedings of ASME Turbo Expo 2023
Turbomachinery Technical Conference and Exposition
GT2023
June 26-30, 2023, Boston, Massachusetts

GT2023-102159

LEARNING RANS MODEL PARAMETERS FROM LES USING BAYESIAN INFERENCE

Santosh Hemchandra[*], **Anindya Datta**
Department of Aerospace Engineering
Indian Institute of Science
Bangalore, 560012, India

Matthew P. Juniper
Department of Engineering
Cambridge university
Trumpington street, Cambridge CB2 1PZ, UK

ABSTRACT

We propose a formal mathematical approach to assimilate LES data into values of RANS model parameters combined with some prior knowledge of the expected RANS parameter values. This is achieved using Bayesian inference to determine parameter values that maximize their posterior probability and is known as maximum a posteriori (MAP) estimation. We apply this approach to a premixed turbulent methane-air round jet flame using unburnt mixture equivalence ratio and bulk flow velocity as design parameters. Three dimesional LES data for six design cases are computed and upto three of these are used for MAP estimation. The likelihood is constructed using RANS solutions and flow statistics from LES at training data points. The k-ε model is used for turbulence closure and the eddy dissipation concept (EDC) model is used to model combustion. RANS solutions using MAP estimate parameters at design points not in the training set show significantly better agreement with LES solutions for species mass fraction and temperature fields while only marginal improvement is observed for velocity fields. We show that assimilating RANS model parameters for both $k-\varepsilon$ and EDC models together yields a higher marginal likelihood than the case that leaves out the EDC model parameters. These results demonstrate the viability of MAP estimation as a means to improving the reliability of turbulent reacting flow RANS simulations for engineering design and optimization applications.

[*]Corresponding author. E-mail: hsantosh@iisc.ac.in

1 INTRODUCTION

Flow through a gas turbine or aircraft engine combustor is typically highly turbulent and includes regions with flames. The reliable prediction of turbulent reacting flow fields, given operating conditions and flow geometry, is important for engineering design and optimization of these devices. Computational Fluid Dynamics (CFD) is a powerful analysis tool that solves the governing equations of turbulent reacting flow on a grid of points in space and time. Methods such as direct numerical simulations (DNS), which resolve the entire range of flow length and time scales, are prohibitively computationally expensive for the design of practical combustors. Accordingly, for practical applications, the class of CFD techniques known as large eddy simulation (LES) is typically used [1]. LES resolves the dynamics of a subrange of the largest flow scale motions in a time accurate manner. Statistics of flow field quantities are then determined by time averaging these solutions. Even LES methods are, however, too computationally expensive for use in practical engineering design optimization methods.

The class of CFD methods based on the Reynolds or Favre averaged Navier–Stokes equations, referred to collectively as RANS, allows the direct prediction of time averaged flow statistics at a significantly smaller computational cost compared with LES. The influence of turbulence is modelled using closure models for turbulent stresses, transport fluxes, and time averaged mean reaction rates. However, since these closure models model the impact of the entire range of flow scales on the time averaged statistics, RANS solutions are more sensitive to changes

in model parameters than LES solutions. Traditionally, RANS model parameters are chosen by comparing RANS predictions of time averaged and/or RMS values of flow field quantities with those from experimental measurements or DNS - see for example [2]. When performed manually, this approach results in RANS model parameters whose predictions may be poor or may not provide correct predictions outside a very narrow range of flow conditions.

Data assimilation of RANS model parameters with Bayesian inference can potentially overcome this problem [3]. These methods incorporate knowledge from LES or experimental measurements into RANS model parameter estimates using Bayes' rule. Importantly, the Bayesian approach allows the uncertainty in the parameter values to be formally estimated and can guide the economical acquisition of additional training data [4]. In the context of gas turbine combustion research, the Bayesian approach to determine model parameters has recently been applied to determine thermoacoustic instability model parameters [5]. Studies using Bayesian inference methods have been applied to infer turbulence model parameters from measurement data for wall bounded non-reacting flows – see for example refs. [6, 7]. Xiao and Cinella [8] review Bayesian inference and other methods for estimating model parameters. To the best of our knowledge, however, attempts at improving flow predictions for reacting flows from steady RANS using data from LES solutions has not been attempted.

In this paper we assess the ability of Bayesian inference to infer RANS model parameters from LES data of a geometrically simple turbulent premixed jet flame [9]. The flow configuration is a premixed methane-air flame at an unburnt gas temperature, $T_u = 800$ K and pressure, $p_o = 1$ atm. Design parameters are the equivalence ratio, ϕ, of the reactant mixture and the nominal inlet velocity on the centreline, U_c. A dataset of five LES solutions, performed using the explicit filtering LES (EFLES) approach for reacting flows described in Datta et al [9], forms the background data for this study. RANS solutions are obtained using the reactingFoam solver implemented using the OpenFOAM solver framework [10]. The $k-\varepsilon$ model [11] and the EDC model [12] are used to close Reynolds stress and mean reaction rate terms.

A prior probability density function (pdf) is used to express prior belief in RANS model parameter values. The likelihood of the LES data for a given choice of RANS model parameters is constructed using the RANS solution for these parameters and time averaged statistics from LES at each training condition. The optimal RANS parameters are then determined as those that maximize the posterior probability of these parameters determined from Bayes' rule. This process involves a formally rigorous optimization of a cost function and is known as maximum a posteriori (MAP) estimation [3, 6, 8].

MAP estimation is applied to a subset of three out of the six LES cases available. The remainder are used to test the accuracy of the optimised RANS model at conditions that are not in the training data. Three model parameters from the $k-\varepsilon$ model and two from the EDC model are used as free parameters for MAP estimation. Additionally, we assess the relative importance of the choice of free parameters used in MAP estimation using the evidence given by marginal likelihood estimates for each choice. These are determined using Laplace's method [3]. The first case varies three parameters in the $k-\varepsilon$ model, while keeping the EDC model parameters at their prior values. The second case includes two additional parameters from the EDC model, giving a total of five free parameters.

2 MAXIMUM A POSTERIORI ESTIMATION

Assume $\mathscr{M}^{RANS}$ is a set of RANS models that are candidates for determining time averaged flow through some geometric configuration under appropriate physical boundary conditions. For a given $\mathscr{H}_p \in \mathscr{M}^{RANS}$, we assume $z \in \mathbb{R}^m$ is an m-dimensional vector of RANS parameters appearing in turbulence closure terms for model $\mathscr{H}_p$. For a given set of design conditions $x \in D$, where D is the design space, the RANS solution for given $z \in \mathbb{R}^m$ is a mapping $y_R(z,x) : D \to \mathbb{R}^N$ where N is the total number of flow variables at fixed set of comparison mesh points $\{r_1, \ldots, r_K\} \in \mathbb{R}^3$. Typically, $y_R(z,x)$ is determined from the solution on the RANS computational mesh using interpolation. Similarly, the LES solution is a mapping $y_L(x) : D \to \mathbb{R}^N$ defined over the same design conditions for the same set of mesh points, $\{r_1, \ldots, r_K\} \in \mathbb{R}^3$. We assume that we have a training set of LES solutions, $Y_{L,N_T} = \{y_{L,1}, \ldots, y_{L,N_T}\}$ where, $y_{L,k} = y_L(x_k)$ for $x_k \in D$. We define the function, $\mathscr{N}(x, \mathbf{A}) = [det(2\pi\mathbf{A})]^{-1/2} \exp(-\frac{1}{2} x^T \mathbf{A}^{-1} x)$, i.e. as the multivariate Gaussian distribution with zero mean and covariance matrix $\mathbf{A}$.

We assume a Gaussian prior on the parameters, z, which is written as:

$$P(z|\mathscr{H}_p) = \mathscr{N}(z - z^*, \mathbf{A}_z) \tag{1}$$

where, $z^* \in \mathbb{R}^m$ are the values of the RANS parameters from prior studies in the literature for a given RANS model, $\mathscr{H}_p$. We presume that the parameters are equally uncertain and uncorrelated and choose $A_z = diag[\sigma_z^2, \ldots, \sigma_z^2]^T$ where, σ_z expresses our prior belief of the uncertainty in z^*. The likelihood distribution of the training data, Y_{L,N_T} being predicted by the RANS model, $\mathscr{H}_p$, for a given choice of parameters, z, is also assumed to be Gaussian:

$$P(Y_{L,N_T}|z) = \prod_{i=1}^{N_T} \mathscr{N}(y_R(z,x_i) - \bar{y}_{L,i}, \mathbf{A}_{L,i}) \tag{2}$$

where, $\bar{y}_{L,i}$ and $\mathbf{A}_{L,i}$ are the time averaged mean vector and diagonal matrix of mean squared fluctuation amplitudes of flow field quantities determined from LES at the design point $x_i \in D$, on the

comparison mesh. The vector $y_R(z,x_i)$ is the flow field prediction from RANS using model parameters z at x_i.

The posterior distribution of z, i.e. the updated *belief* in the numerical values of model parameters z, given the training data $Y_{L,NT}$, is determined using Bayes' rule:

$$P(z|Y_{L,N_T}) = \frac{P(Y_{L,N_T}|z)P(z|\mathscr{H}_p)}{P(Y_{L,N_T}|\mathscr{H}_p)} \tag{3}$$

Maximizing $P(z|Y_{L,N_T})$ over $z \in \mathbb{R}^m$ yields optimal RANS parameters, i.e. those that are associated with high belief, given the training LES data. These parameters are referred to as the maximum a posteriori (MAP) estimate and can be determined as follows. Taking the logarithm of both sides of eq. 3 and rearranging yields,

$$\begin{aligned} -\log[P(Y_{L,N_T}|\mathscr{H}_p)] =& \log[P(z|Y_{L,N_T})] \\ &- \log[P(z|\mathscr{H}_p)] \\ &- \log[P(Y_{L,N_T}|z)] \end{aligned} \tag{4}$$

The quantity on the left of eq. 4 is a constant, independent of z. Therefore, maximizing the posterior probability (or equivalently, its logarithm), is equivalent to minimizing the sum of the second and third terms on the right in eq. 4, i.e. the sum of the negative logarithms of the prior and likelihood. Using the expressions for the prior (eq. 1) and likelihood (eq. 2) in the second and third terms on the right in eq. 4, yields the cost function that must be minimized to determine the MAP estimate z_{MAP}:

$$\begin{aligned} J(z) =& (z-z^*)^T \mathbf{A}_z^{-1}(z-z^*) + \log[\det(2\pi\mathbf{A}_z)] \\ &+ \sum_{i=1}^{N_T} [y_R(z,x_i) - y_{L,i}]^T \mathbf{A}_{L,i}^{-1} [y_R(z,x_i) - y_{L,i}] \\ &+ \sum_{i=1}^{N_T} \log[\det(2\pi\mathbf{A}_{L,i})] \end{aligned} \tag{5}$$

If z_{MAP} is defined as $\min_{z\in\mathbb{R}^m} J(z)$, then the uncertainty in z_{MAP} to leading order is determined using Laplace's method [3], which approximates the posterior distribution of z around z_{MAP} using the Taylor expansion of $\log[P(z|Y_{L,N_T})]$:

$$P(z|Y_{L,N_T}) \approx C \exp\left[-\frac{1}{2}(z-z_{MAP})^T \mathbf{H} (z-z_{MAP}) \right] \tag{6}$$

where $\mathbf{H}$ is the Hessian of the cost function $J(z)$ at $z = z_{MAP}$: $H_{ab} = [\partial^2 J/\partial z_a \partial z_b]|_{z=z_{MAP}}$ and C is a constant.

At the next level of inference, the marginal likelihood of the data, Y_{L,N_T} for a given a RANS model, $\mathscr{H}_p$, is calculated. This is the denominator of eq. 3:

$$P(Y_{L,N_T}|\mathscr{H}_p) = \int_{\mathbb{R}^m} P(Y_{L,N_T}|z)P(z|\mathscr{H}_p)\, dV(z) \tag{7}$$

The marginal likelihood quantifies the evidence that the RANS model $\mathscr{H}_p$ predicts the data Y_{L,N_T}. The integrand in eq. 7 can be written using eqs. 4 and 5 as $\exp[-(1/2)J(z)]$. Using the Taylor expansion of $J(z)$ around $z = z_{MAP}$ (Laplace's method), the marginal likelihood can be estimated as [3],

$$P(Y_{L,N_T}|\mathscr{H}_p) \approx P(Y_{L,N_T}|z_{MAP})P(z_{MAP}|\mathscr{H}_p)\det(\mathbf{H}/2\pi)^{-1/2} \tag{8}$$

Thus combining eqs. 8 and eq. 5, the negative log evidence (NLE) can be written as follows

$$NLE = J(z_{MAP}) + \log[\det(\mathbf{H}/2\pi)] \tag{9}$$

Thus RANS models can be compared in terms of their ability to predict the data, i.e. given a set of candidate models $\mathscr{M}^{RANS}$, the model $\mathscr{H}_p \in \mathscr{M}^{RANS}$ having the least NLE for a given number of training data points, Y_{L,N_T}, is the most likely predictor of the data .

3 LARGE EDDY SIMULATION

The test case studied in this paper is a turbulent round premixed methane air flame, shown schematically in fig. 1. Fully three dimensional computations are performed for an unburnt gas temperature $T_u = 800$ K and operating pressure of 1 atm, on a cylindrical domain as shown in fig. 1. The jet diameter, $D = 2.0$ mm and the origin of co-ordinates is on the centerline of the jet at the dump plane. The inlet is positioned upstream of the dump plane at $z/D = -1$. The design parameters for this study are, $x = [\phi\ U_c]^T$, where, ϕ is the upstream equivalence ratio and U_c is the jet centreline inflow velocity.

LES is performed in this study at design conditions summarized in tab. 1 and plotted in design space in fig. 2. Solutions for cases 1-3 in tab. 1 are used as training data for MAP estimation and solutions for cases 4-6 are used as test data. The latter are used to determine how well the RANS model with MAP estimate values for model parameters determined from training data, extrapolates to other design points.

LES solutions are obtained using the explicit filtering LES (EFLES) method for reacting flows initally proposed by Mathew and co-workers [13, 14] for non-reacting flow and extended to the reacting flows by Datta et al [9]. Note that case 1 in tab. 1 is the same case as in their study. The EFLES method solves

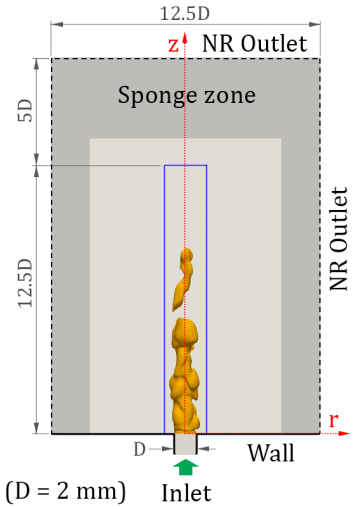

FIGURE 1: Schematic of Burner Configuration. An instantaneous iso-contour of progress variable (based on O_2 mass fraction) c = 0.65 is shown ($\phi = 0.8$, $U_c = 65$ m/s, $T_u = 800$ K). The blue box shows the mesh region that nominally contains the flame.

Sl. num.	ϕ	U_c (m/s)
1	0.80	65.0
2	0.80	68.0
3	0.76	64.0
4	0.84	52.0
5	0.88	60.0
6	0.72	56.0

TABLE 1: Design conditions at which LES solutions are obtained for data assimilation.

the governing equations for reacting flow by first advancing the flow state through a timestep without including terms for subgrid scale models and captures the impact of these by spatially low-pass filtering the result [9]. Chemical source terms are computed using the resolved scale species and temperature fields with a reduced order chemical kinetic model for methane-air combustion, proposed by Sankaran et al [15]. Datta et al [9] have shown that EFLES recovers flow statistics variations in good agreement with a fully resolved direct numerical simulation (DNS) for case 1 in tab. 1. We refer the reader to their paper for full details of how EFLES is mathematically derived and quality of agreement between LES and DNS for case 1. Here, we briefly summarize details of the numerical method and flow setup.

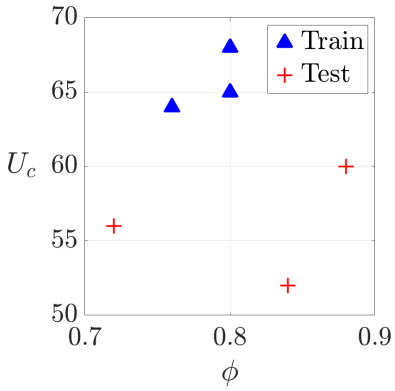

FIGURE 2: Conditions in design space at which LES solutions are obtained. Triangles are training cases and pluses are cases used for testing.

The flow solver integrates the governing equations of compressible reacting flow in a time accurate manner. Computations are performed using the strong conservation form of the flow govering equations on structured multiblock meshes – see for example Visbal and Gaitonde [16]. Spatial flux derivatives are computed using eighth order explicit central differences and time integration is performed using a third order Runge-Kutta scheme [17]. Spatial filtering required to realise EFLES is performed using a tenth order symmetric shift-invariant filter, as described in Datta et al [9]. The domain shown in fig. 1 is discretized using a computational mesh with $\sim 480,000$ mesh points. The flame length and velocity scales at the nominal condition given by case 1 in tab. 1 are: nominal flame speed, $s_L = 2.05$ ms^{-1}; thermal thickness[1], $\delta_L = 300$ μm; heat release zone thickness,[2] $\delta_H = 120$ μm, and burnt gas temperature, $T_b = 2313.65$ K. The mesh size within the blue box shown in fig. 1 is ~ 180 μm $= 1.5\delta_H$.

Walls are treated using no-slip boundary conditions with a specified temperature profile. This profile rises smoothly from $T_u = 800$ K at the inlet boundary to T_b on the dump plane. Non-reflecting boundary condition treatments are applied at boundaries downstream of the dump plane. All boundary conditions are implemented using the Navier–Stokes characteristic boundary conditions method [18]. Additionally, sponge zones [19] shown schematically in fig. 1, are used to damp out vortices and pressure waves ahead of the downstream boundary. A top hat mean axial velocity profile with a centerline value of U_c from tab. 1 is applied in each case. These correspond to flow Reynolds numbers, $Re \sim U_c D/\nu \sim 1500$. Additionally, diver-

[1] Computed from 1D premixed flame temperature profile based on maximum temperature gradient, $\delta_L = (T_b - T_u)/(dT/dx)_{max}$

[2] Estimated as the full width at half maximum (FWHM) of the nominal 1D premixed flame heat release rate layer

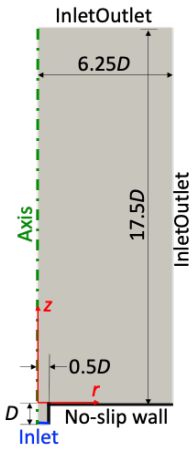

FIGURE 3: Domain used for RANS modelling of the turbulent jet flame. The blue box shows the region used to determine the likelihood of the RANS solutions against LES training data.

gence free synthetic turbulence inflow fluctuations are imposed in order to realize a turbulent upstream reactant flow at these *Re* values. These fluctuations are precomputed so as to conform to a Von Karman-Pao energy spectrum and advected into the inflow plane during LES runs assuming Taylor's hypothesis. The DNS solution for case 1 from the work of Datta et al [9], yields turbulent Reynolds and Karlovitz numbers as 34 and 25 respectively. These values are nominal and place the flames in cases 1-6 in tab. 1 within the thin reactions zone regime of premixed combustion.

All cases were advanced in time for five complete flow through times from the dump plane to the downstream outlet boundary. The final three flow through times were used to collect statistics of various flow field quantities. Each LES case took a total of $\sim$ 5000 core-hours of compute resources and were performed on the high performance compute facility in the department of Aerospace engineering at the Indian institute of science.

4 RANS MODELLING

Steady Reynolds averaged Navier-Stokes (RANS) simulation is viewed in this paper as a model that predicts mean flow field quantities directly given the domain geometry and boundary conditions. For the present flow configuration, in which time averaged statistics are axi-symmetric, a significant reduction in computational effort is achieved by performing 2D axi-symmetric RANS computations. Accordingly, the domain used for RANS simulations is the area of rotation that generates the cylindrical LES domain as shown in fig. 3. Computations are performed using the *reactingFoam* solver available with the OpenFOAM v2206, open source CFD software suite [10]. The nozzle is discretised with 20 cells radially and 35 cells axially. The domain downstream of the dump plane is discretized using 85 cells radially and 175 cells axially. The whole domain is one cell thick in the out of $r-z$ plane direction. The mesh is compressed towards the dump plane wall and the nozzle wall to resolve spatial gradients of flowfield quantities in these regions. Increasing mesh resolution or domain width downstream of the dump plane resulted in negligible changes in convereged steady state flow field quantities. The standard $k-\varepsilon$ model is used to close the Reynolds stress terms [11] and the EDC model based on the energy cascade model of Magnussen [12] is used to determine time averaged chemical source terms – see Parente et al [2] for additional discussion.

The boundary conditions imposed on the domain boundaries are summarized in fig. 3. The time averaged inflow velocity profile is specified using the same top hat profile as in the LES cases, using the hyperbolic tangent function. A constant inflow turbulent kinetic energy (TKE) intensity of 0.35 is imposed on this boundary to match the turbulence level specified in the LES. No-slip boundary conditions are specified on the inlet pipe and dump plane walls. Constant wall temperatures of 800 K and adiabatic flame temperature on the inlet pipe and dump plane walls respectively, are specified. An inlet/outlet treatment is applied at downstream and lateral boundaries for all flow field variables, with inlet values specified as the burnt gas temperature and composition. These values are imposed by the RANS solver whenever the local fluxes on the boundary cells point into the domain.

The standard $k-\varepsilon$ model closes Reynolds stress terms using an eddy viscosity closure. The eddy viscosity is defined using the TKE, k and viscous dissipation rate, ε as $\nu_t = C_\mu(k^2/\varepsilon)$. The turbulent kinetic energy equation is solved for k, wherein the sink term is written in terms of ε and an additional model transport equation is introduced for ε. The strength of the production and dissipation terms in the ε equation are adjusted using parameters $C_{1\varepsilon}$ and $C_{2\varepsilon}$ respectively. We note here that it is well known that additional terms capturing the physical impact of flow three-dimensionality, eg. vortex stretching, must be added to the standard $k-\varepsilon$ model equations to correctly recover the spreading rates of round jets [20–22]. The current implementation of turbulence models available in the reactingFoam solver used in this work do not directly provide an option to include these terms. However, the main aim of this paper is to demonstrate and assess the improvement on RANS predictions that can be obtained using MAP estimation to assimilate data in model parameters for a reacting flow. Therefore, extending the formulation of the $k-\varepsilon$ model in the reactingFoam solver was not included within the scope of this study.

The mean reaction rate is modelled using the eddy dissipation concept (EDC) model of Magnussen [12]. The EDC models combustion occurring within fine structures embedded within the turbulent flow, as being approximated by perfectly stirred reactors. The local mass fraction of these fine structures, γ_λ and the mean residence time within them τ^* are modelled in terms of the

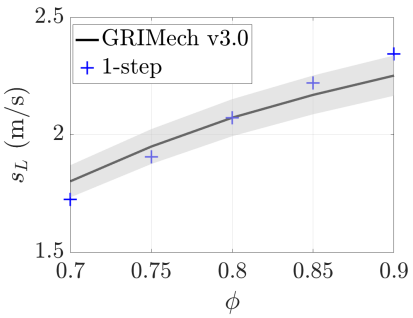

FIGURE 4: Comparison between bf new 1-step (symbols) and GRI-Mech 3.0 (curve) predictions of laminar flame speed for methane-air ($T_u = 800$ K, $p = 1$ atm). The grey band shows a 3% error band around the predictions from GRI-mech 3.0.

local k and ε values as follows [2, 12],

$$\gamma_\lambda = C_\gamma \left(\frac{\nu \varepsilon}{k^2} \right)^{1/4} \tag{10}$$

and

$$\tau^* = C_\tau \left(\frac{\nu}{\varepsilon} \right)^{1/2} \tag{11}$$

where, C_γ and C_τ are model constants. We model chemical kinetics in the RANS simulations using a single step bimolecular global reaction: $CH_4 + 2O_2 \rightarrow CO_2 + 2H_2O$, with a global rate given by, $\dot{\omega} = A \exp(-E_a/RT)[CH_4]^{1/2}[O_2]$ where, $A = 6.4 \times 10^{12}$ $(\text{mol cm}^{-3})^{-2}\ \text{s}^{-1}$, $E_a = 41.27$ kcal mol^{-1} and R is the universal gas constant. These parameters recover the laminar flame speed of a freely propagating methane-air flame to within at least 3% of that predicted by the detailed GRI-Mech 3.0 mechanism [23], across the range of ϕ values spanned by the cases in the LES study (tab. 1) - see fig. 4.

Thus, the model parameter vector for MAP estimation can be written as: $z = [C_\mu\ C_{1\varepsilon}\ C_{2\varepsilon}\ C_\gamma\ C_\tau]^T$. These model parameter values have been determined in previous studies using methods that minimize the discrepancy between measurements and RANS predictions. It is easy to see from eq. 2 that this approach is equivalent to finding parameters that maximise the likelihood of the data. As such they may be referred to as the maximum likelihood estimate (MLE) of the parameters. The MLE approach to determining parameter values is known to suffer from problems of "overfitting", wherein the parameters determined predict the training data but can cause the model to extrapolate poorly [3]. MAP estimation mitigates this by allowing for the incorporation of prior insight when determining parameters. A key difference between MLE and MAP is that while the former maximises the likelihood of the data, the latter determines parameters that have highest probability, given a model choice and training data. The key aim of this paper is to assess the improvement in RANS predictions achieved by maximising the posterior probability of parameters given data. Accordingly, we assume the following well known parameter values [2, 11], as the mean of the prior distribution (see eq. 1):

$$z^* = [0.09\ \ 1.44\ \ 1.92\ \ 2.13\ \ 0.41]^T \tag{12}$$

An arbitrary variance of 2 for each of the values in eq. 12 is assumed to construct the prior pdf. Note that, from eq. 5, this value determines the contribution from the negative log of the prior to the overall cost function and therefore controls the strength of the penalization imposed by the prior on the MAP estimate, z_{MAP}. Choosing a small value for the prior variance implies a high degree of belief in these values and can result in poor quality of the match between LES and RANS solutions for $z = z_{MAP}$. Too large a value of prior variance would undermine the penalization imposed by the prior on the value of $J(z)$ and would result in the re-emergence of overfitting.

The LES and RANS solutions are interpolated onto a uniform equispaced mesh with 41 points in the axial direction and 8 points in the radial direction in a rectangular region between $0 < z/D < 10$ and $0 < r/D < 1.5$. We will refer to this mesh as the *comparison* mesh. The model prediction $y_R(z, x_k)$ and data $y_{L,k}$ for the i^{th} training case in eq. 5, are the vector of axial velocity, temperature and species mass fraction fields on comparison mesh points, as determined from the RANS and LES solutions. The covariance matrix of the likelihood function (eq. 2) is constructed using the mean squared fluctuation amplitudes of flow field quantities interpolated from LES solutions at comparison mesh points.

A typical LES result (case 1: $\phi = 0.8$, $U_c = 65$ m/s) showing the spatial extents of the flame brush is shown in fig. 5a. Spatial distributions of root mean square (RMS) fluctuation amplitudes of temperature (T') and axial velocity ($u'_{z,RMS}$) are shown in fig. 5b-c for this case. Comparing these results shows that T' and $u'_{z,RMS}$ amplitudes are very small outside the flame brush and jet core region. Therefore, using these fields directly to determine data uncertainties in eq. 5 will result in larger contributions to the net likelihood from points outside the flame brush and jet core, than from those within. This will in turn, bias the minimization towards parameter values that yield RANS solutions that agree better outside the flame brush and jet core, rather than within. Therefore, for each solution field, a threshold RMS fluctuation amplitude value of half of its maximum value on the comparison mesh is used to identify masked points and the RMS fluctuation amplitude at these points is set to 1.1 times the maximum value. The masked RMS fields are smoothed using Gaussian filtering to ensure smoothness of the resulting MAP cost function. Fig-

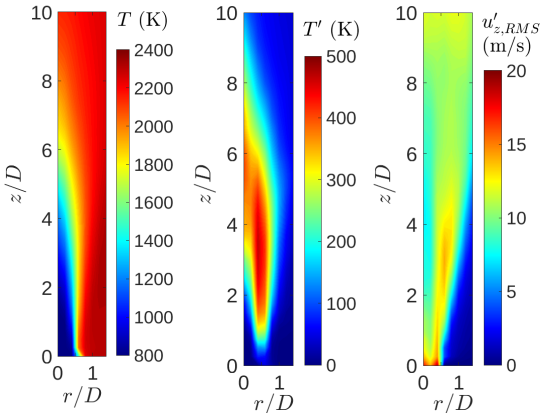

FIGURE 5: Typical spatial variation of the contribution from the temperature field to the likelihood from LES for case 1 ($\phi = 0.8$, $U_c = 65$ m/s, a) Mean b) RMS (raw) c) RMS (masked). Data is plotted on the comparison mesh.

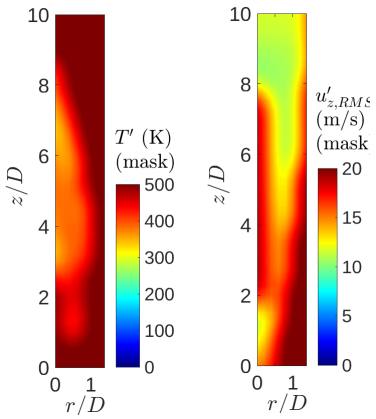

FIGURE 6: Typical spatial variations of masked RMS fields from LES for case 1 ($\phi = 0.8$, $U_c = 65$ m/s), used to determine the likelihood of RANS solutions, a) T b) $u'_{z,RMS}$. Data is plotted on the comparison mesh

ure 6a-b shows the masked T' and $u'_{z,RMS}$ fields corresponding to the RMS fields shown in fig. 5b-c. Using these masked fields to define data uncertainties in eq. 5 now ensures that contributions to the likelihood from points within the flame brush dominate the net value of the MAP cost function. This treatment ensures that the minimization will now select model parameters that prioritise agreement between RANS and LES solutions within the flame brush. More generally, when applying the present method to other classes of flows, similar masking may be used to identify important flow field regions where good prediction accuracy is needed from RANS solutions.

Minimization of the MAP cost function ($J(z)$, eq.5) is performed in two stages. The first stage is performed using the implementation of the Nelder-Mead simplex algorithm [24] provided by the `fminsearch` function in the MATLAB optimization toolbox. This algorithm is a gradient-free minimization algorithm that determines an estimate of the minimizer of $J(z)$ without using function gradients. A final gradient based optimization is performed using the implementation of the interior-point algorithm provided by the `fmincon` function in MATLAB. Gradients of $J(z)$ are computed using central second order finite-differences in parameter space. The use of `fmincon` also allows for a search region in parameter space to be specified by imposing upper and lower bound constraints on parameter values. The minimum found in this step is verified to lie within the interior of the search region.

All RANS solutions are initiated from a baseline converged solution obtained from an arbitrary initial guess using the prior parameters z^*. The RANS iterations were continued until the global maximum residual of all equations was below 3×10^{-5}. This value was sufficient to ensure the smoothness of $J(z)$ over the space of parameter values encountered during both minimization stages. The approximate Hessian returned by the final gradient based minimization stage is used in eq. 6 to determine the uncertainty in the MAP estimate of the parameters. The entire MAP minimization run using three LES data points and five RANS model parameters took two days of run time on a single core of a typical workstation desktop computer.

5 RESULTS AND DISCUSSION

We first compare LES and RANS solutions obtained using parameter values z^*. Note that this amounts to making model predictions with only prior information and not accounting for any data. Figure 7a-d shows a typical result comparing time averaged fields from LES and RANS solutions for LES case 4 (see tab. 1, $\phi = 0.84$, $U_c = 52$ m/s). Note from fig. 2 that this point is farthest in design space from the three cases selected for training. The RANS and LES results are shown on the left and right halves of each figure respectively. Since the flame is nominally axisymmetric, qualitative agreement between RANS and LES solutions can be assessed by comparing left and right halves of each figure. The solid magenta contours in figs. 7a-c show $\bar{c} = 0.5$ contours, where, $\bar{c}$ is defined for each of $\bar{Q} = T, \bar{Y}_{CH_4}, \bar{Y}_{H_2O}$, using their values in the burnt ($\bar{Q}_b$) and unburnt ($\bar{Q}_u$) gas in the LES results as, $\bar{c} = (\bar{Q} - \bar{Q}_u)/(\bar{Q}_b - \bar{Q}_u)$. The broken magenta curves in figs. 7a-c are $\bar{c} = 0.5$ contours corresponding to $\bar{Q} \pm Q'_{RMS}$ in each case, where, Q'_{RMS} is the raw RMS field from LES. These curves show the uncertainty in the spatial position of the $\bar{c} = 0.5$ contour in each case.

Comparing the RANS and LES predictions in fig. 7a-d shows poor agreement to varying levels across all fields. The

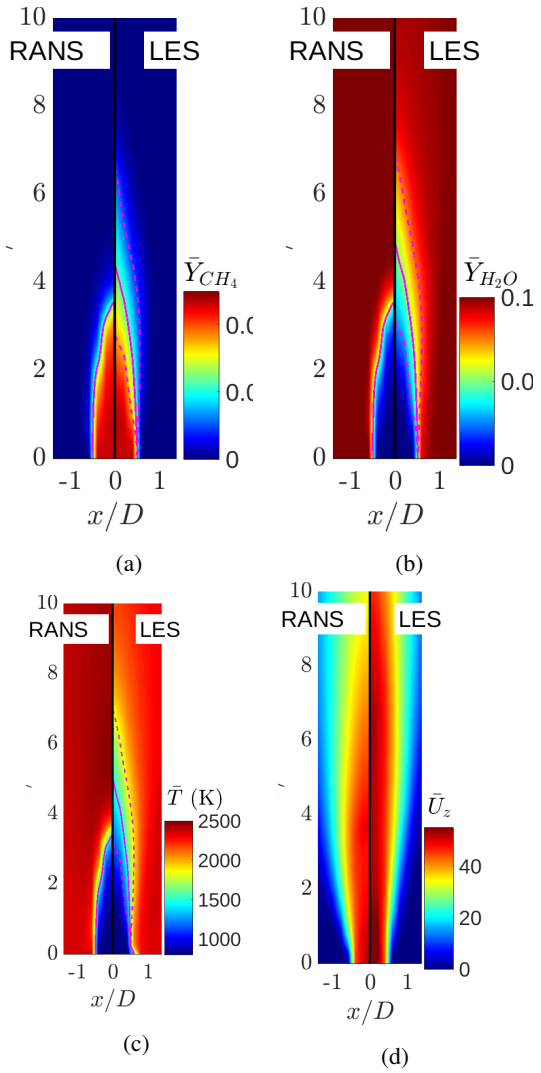

FIGURE 7: Typical comparison between time averaged RANS and LES solutions for LES case 4 ($\phi = 0.84$, $U_c = 52$ m/s) using RANS model parameter values suggested by the prior, (a) $\bar{Y}_{CH_4}$ (b) $\bar{Y}_{H_2O}$ (c) $\bar{T}$ (d) $\bar{U}_z$. The left half of each figure shows the RANS result and the right half shows the time averaged LES result.The solid magenta curves in (a-c) show mean progress variable $\bar{c} = 0.5$ contours. The broken magenta curves on LES results in (a-c) show $\bar{c} = 0.5$ contours for fields separated by one standard deviation from the mean field. Data is plotted on the comparison mesh

vertical extent of the $\bar{c} = 0.5$ contours may be interpreted as a measure of the flame height. It is clear from fig. 7a-c that the predicted flame height is shorter in the RANS simulations than the LES. In addition, the flame brush width is significantly thinner in the RANS results than in the LES. Both of these characteristics may be attributed to the choice of the 1-step mechanism in the

Data	C_μ	$C_{1\varepsilon}$	$C_{2\varepsilon}$	C_γ	C_τ	$\|\|\nabla_z J/J\|\|_\infty$
-	0.09	1.44	1.92	2.13	0.41	-
1	0.078	1.69	1.51	2.13	0.41	0.036
1	0.098	1.35	1.99	1.16	0.59	0.016
1-3	0.099	1.36	1.97	1.19	0.6	0.035

TABLE 2: RANS model parameter values determined from MAP estimation. Grayed out cells show parameters that were held fixed at prior values z^* (eq.12), during cost function minimization.

RANS which does not allow for product dissociation. This also results in a higher burnt gas temperature in the RANS as fig. 7c shows. The RANS results for species mass fractions in fig. 7a-b also consistently show thinner flame brushes. Figure 7d shows that the spatial distribution of $(\bar{U}_z)$ spreads more rapidly with increasing downstream distance along the centreline in the RANS solutions when compared with the LES result. This is consistent with past studies that have reported similar behaviour in non-reacting jets [20, 22] and is due to the absence of terms capturing the impact of three dimensional flow in the standard $k-\varepsilon$ RANS model, as discussed earlier. The same effect is reflected here in our reacting flow simulations using RANS. The inherently three dimensional nature of our LES computations, implicitly captures these physics. Results from other cases in tab. 1 resemble those in fig. 7 and are not shown.

Table 2 lists model parameters obtained using MAP estimation. In each row, grayed out cells show parameters that were held fixed at their prior values during MAP estimation. We refer to those parameters included in MAP estimation as free parameters. The first column summarizes the composition of the training dataset used in each case. Accordingly, the first row lists parameter values, z^* (eq. 12), from the prior. The numbers in the first column in rows 2-4, correspond to LES case numbers given in tab. 1. Comparing row 1 with those in other rows in tab. 2, shows that introducing even one training data point significantly changes the MAP estimate of some model parameter values. Rows 2 and 3 show that increasing the number of free model parameters to include those of the EDC model, in addition to the $k-\varepsilon$ model, results in a significant change in EDC model parameter values. The change in parameter values is marginal with inclusion of additional training data, however, as can be seen by comparing rows 3 and 4 in tab. 2. Overall, comparing parameter values in row 4 with row 1 shows that the EDC model parameters and the ε-equation source term parameter, $C_{1\varepsilon}$ show the most significant changes from their prior values. The reduction in $C_{1\varepsilon}$ broadly reduces values of ε in the flow solution which then causes the local eddy viscosity within the framework

Data	Free parameters	$[det(\mathbf{H})]^{-1/2}$	*NLE*	*NNLE*
-	None	32.0	-	-
1	$k-\varepsilon$ only	1.086	489.4	489.4
1	$k-\varepsilon$, EDC	0.43	380.2	380.2
1-3	$k-\varepsilon$, EDC	0.014	1210.4	403.5

TABLE 3: Parameter uncertainty and negative log evidence (*NLE*) of MAP model parameter estimates in tab. 2. *NNLE* is the *NLE* per training data point.

of the $k-\varepsilon$ model to increase. The reduction in C_γ and the increase in C_τ implies that the mass fraction of reaction carrying fine scale structures in the flow reduces while the flow residence time within these structures increases. Both of these facts diminish the time averaged chemical source term value from that predicted by using parameters from the prior. We will verify that both these effects result in a broadening of the flame brush later in this paper

At this level of inference, neither the impact of including additional training data nor the appropriate choice of free model parameters for MAP estimation are immediately obvious. The first of these is addressed by using Laplace's method to examine the change in uncertainty estimates of the MAP values. The second is addressed by examining the change in *NLE* estimates (eq. 9) for each case. Table 3 lists uncertainties, negative log evidence (*NLE*) and *NLE* per training data point, *NNLE* for each of the three training datasets listed in tab. 2. The uncertainty in each set of MAP estimate model parameters is quantified by $[det(\mathbf{H})]^{-1/2}$. This number, up to a constant factor, determines the volume of the unit standard deviation ellipsoid around the MAP estimate in parameter space. A first significant reduction in model parameter uncertainty is obtained by assimilating data, as comparing values of $[det(\mathbf{H})]^{-1/2}$ between the first and remaining rows in column 3 of tab. 3 shows. A further reduction is achieved by including EDC model parameters in the estimation – see rows 2 and 3 in column 3 of tab. 3. Including additional training data increases the uncertainty in model parameters as comparing values in rows 3 and 4 in tab 3 shows. This may just be due to the somewhat higher value of the cost function gradient for this case from tab. 2 when compared to the single training point case. This was the best possible value achieved within the scope of the present study. Using adjoint solutions to determine the gradient of $J(z)$ can potentially improve the MAP estimate. Implementing this however, is beyond the scope of the present study. Nevertheless, the progressive reduction in uncertainty of the MAP estimate relative to the prior, is typical when using Bayesian inference, as the addition of data results in a readjustment of prior beliefs about model parameter values.

The fourth column in tab. 3 lists the negative log evidence (*NLE*) for each choice of model parameters and data. Note that a lower value of *NLE* implies increased probability that the data is predicted by the choice of the model, characterised in this case by the choice of free parameters. Comparing *NLE* values in rows 2 and 3 shows that including EDC parameters reduces the NLE evidence - suggesting that the choice of five free parameters from the $k-\varepsilon$ and EDC models yields the appropriate model, consistent with what physical intuition would suggest. The higher *NLE* in row 4 for the case with three training data points when compared to the case with a single training point in row 3 is simply a reflection of the increase in the number of training points as in both of these cases, the free parameters are identical. This is shown by the marginal change in the value of *NNLE* in rows 3 and 4 in tab. 3.

We now compare predictions at test point 4 in tab. 1 using MAP estimate RANS model parameters from row 4 in tab. 2. Results comparing RANS and LES results for case 4 in tab. 1 are presented in fig. 8 in exactly the same manner as those shown in fig. 7 (see appendix A for similar results for other cases in tab. 1). Comparing the two sets of results shows that the quality of agreement between RANS and LES for temperature and species mass fraction fields has significantly improved - even at a test case that wasn't part of the training data - see fig. 2. The $\bar{c}=0.5$ contours in the RANS solutions now lie well within the band of uncertainty around the time averaged LES data and show a flame brush that compares better with the LES as figs. 8a-c show. The broader flame brush in the RANS results in figs. 8a-c is a consequence of increased turbulent viscosity and smaller time averaged chemical source term values predicted by the MAP estimate model parameters.

Figure 9a-d shows typical radial profiles at an axial position of $z/D=4$ from RANS and LES solutions for test case 4 ($\phi=0.84$, $U_c=52$ m/s, see tab. 2). The unit standard deviation uncertainty band around the LES result (curve) is shown in grey. Results from RANS solutions using prior (crosses) and MAP estimate (filled circles) model parameters from row 4 in tab 2 are overlaid for comparison. These results are typical and similar trends are seen for traning cases and test cases 5 and 6 in tab. 1 as well. Thus, it is clear from fig. 8 and 9 that for temperature and species mass fraction fields, using MAP parameters, considerably improves the quantitative accuracy of the RANS when compared to results obtained using parameters suggested by the prior alone. Figure 9d shows that the improvement in the change of jet spreading rate in the RANS and LES results for $\bar{U}_z$ is marginal, consistent with results in figs. 7d and 8d. These results again show the importance of additional terms in the $k-\varepsilon$ model suggested by Pope [20] and Sarkar and Lakshmanan [21] is essential to improve the quantitative predicition of the jet spreading rate in the RANS [22].

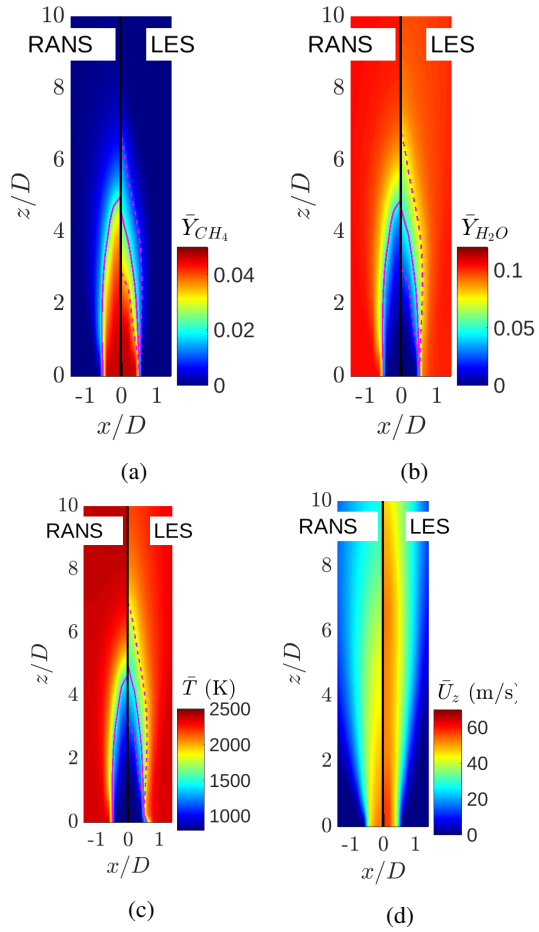

FIGURE 8: Typical comparison between time averaged RANS and LES solutions for LES case 4 ($\phi = 0.84$, $U_c = 52$ m/s) using MAP estimate RANS model parameter values, (a) $\bar{Y}_{CH_4}$ (b) $\bar{Y}_{H_2O}$ (c) $\bar{T}$ (d) $\bar{U}_z$. In each figure, the left half shows the RANS result and the right half the time averaged LES result. The solid magenta curves in (a-c) show mean progress variable $\bar{c} = 0.5$ contours. The broken magenta curves on LES results in (a-c) show $\bar{c} = 0.5$ contours for fields separated by one standard deviation from the mean field. Data is plotted on the comparison mesh.

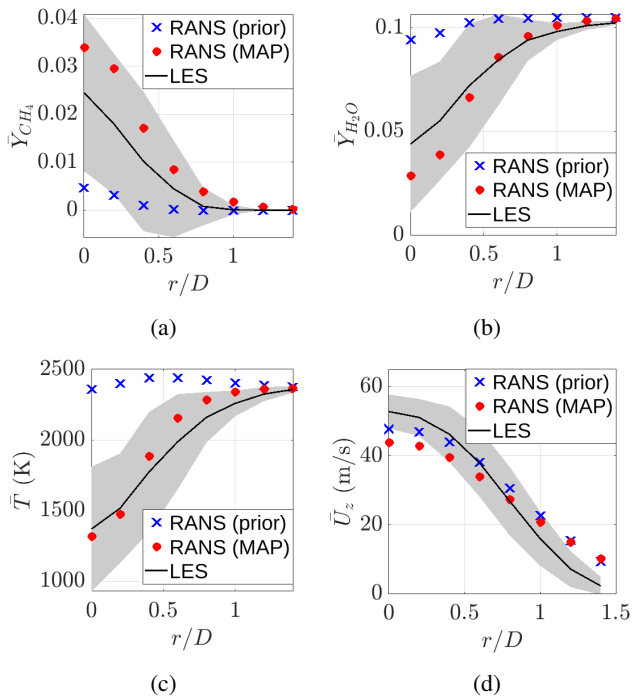

FIGURE 9: Typical Radial profiles of flow field quantities at $z/D = 4$ from RANS and LES solutions for test case 4 ($\phi = 0.84$, $U_c = 52$ m/s), (a) $\bar{Y}_{CH_4}$ (b) $\bar{Y}_{H_2O}$ (c) T (d) U_z. The unit standard deviation uncertainty band around the LES is shown in grey. Data is plotted at comparison mesh points

6 CONCLUSIONS

This paper demonstrates the use of Bayesian inference to assimilate training data from large eddy simulation (LES) into closure model parameters for Reynolds averaged Navier-Stokes (RANS) simulations. The configuration chosen for this study is a turbulent round jet flame at flow Reynolds number, $Re \sim 1500$. Inflow forcing by synthetic turbulence sustains a turbulent flow ahead of the flame. The design parameters of the problem, upstream equivalence ratio and bulk axial flow velocity, are varied in the range $0.7 - 0.9$ and $50 - 70$ m/s respectively. The upstream reactant temperature is held fixed at $T_u = 800$ K. LES is performed using the explict filtering LES (EFLES) method described in Datta et al [9]. Steady RANS computations of the same configuration are performed in a 2D-axisymmetric configuration using the reactingFoam flow solver, as provided, with openFoam libraries and tools [10]. The $k - \varepsilon$ model is used to close Reynolds stress terms and the eddy dissipation concept (EDC) model is used to model the time averaged reaction rate.

RANS model parameters are determined using maximum a posteriori (MAP) estimation. Mathematically, prior belief in numerical values for RANS model parameters is expressed as a Gaussian pdf over parameter space with mean parameter values from previous studies and variance chosen arbitrarily. The likelihood of the data for a given choice of parameters is constructed from the corresponding RANS solution combined with flow statistics from LES. The most likely model parameter values are taken to be those that have the maximum posterior probability. This is determined using Bayes' theorem by minimizing a cost function, which is the negative log likelihood of the posterior probability. The Hessian of this cost function at the MAP estimate provides a leading order approximation to the posterior pdf around the MAP parameter values using Laplace's method [3]. This allows quantification of the uncertainty in the MAP esti-

mate parameter values and also the marginal likelihood that the LES data is predicted by the RANS model.

Our results show that, for this flow configuration, assimilating RANS model parameters with MAP estimation significantly improves agreement between RANS and LES solutions for the mean species mass fractions and the temperature, even for cases at design parameters that were not part of the training data. The absence of terms capturing turbulence effects resulting from three dimensionality of the turbulence field in the $k-\varepsilon$ model equations implemented within reactingFoam results in increased jet spreading rates in the RANS simulations, when compared with LES. Including these terms can therefore improve RANS predictions of the velocity field as well. This is an important point to be addressed in future work. Note that the inherently three dimensional nature of our LES computations captures this physics.

Model parameter uncertainty estimates show that inclusion of additional training data and EDC model parameters, in addition to those of the $k-\varepsilon$ model, as free parameters in MAP estimation, reduces the uncertainty of the MAP estimate. Also, the increase in marginal likelihood when EDC model parameters are included in MAP estimation provides evidence that the five parameter model is the appropriate model that can explain the data. In summary, all of these results demonstrate the validity of using MAP estimation as a means of improving the reliability of RANS predictions using LES for the present flow configuration. This provides confidence that similar results can be achieved for flows at higher *Re* in and in realistic configurations. The MAP estimation method formulated in this paper is general and can be easily applied to any LES and RANS solver combination.

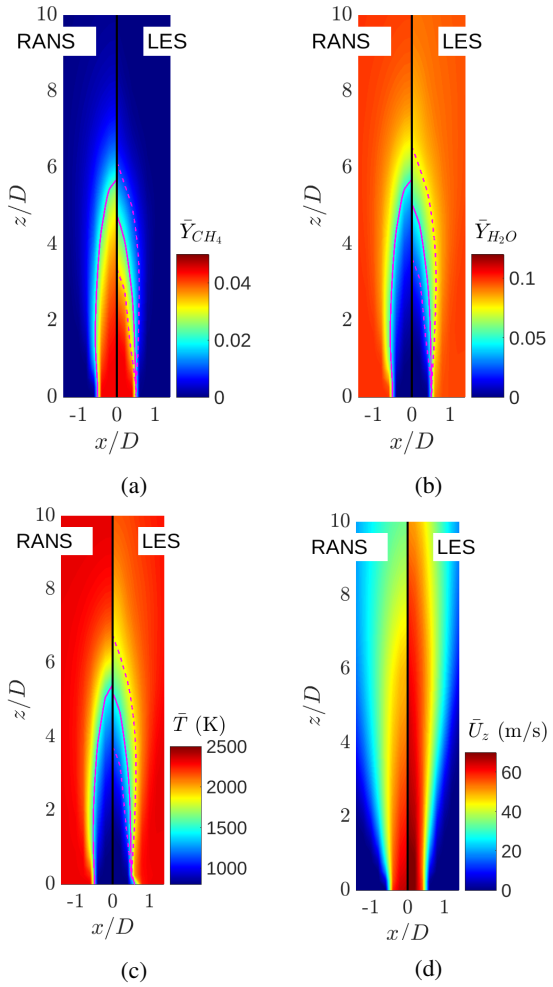

FIGURE 10: Typical comparison between time averaged RANS and LES solutions for LES case 1 ($\phi = 0.8$, $U_c = 65$ m/s) using MAP estimate RANS model parameter values, (a) $\bar{Y}_{CH_4}$ (b) $\bar{Y}_{H_2O}$ (c) $\bar{T}$ (d) $\bar{U}_z$. In each figure, the left half shows the RANS result and the right half the time averaged LES result. The solid magenta curves in (a-c) show mean progress variable $\bar{c} = 0.5$ contours. The broken magenta curves on LES results in (a-c) show $\bar{c} = 0.5$ contours for fields separated by one standard deviation from the mean field. Data is plotted on the comparison mesh.

ACKNOWLEDGEMENTS

SH gratefully acknowledges support from Trinity College Cambridge as a Visiting Fellow. Several useful discussions with Matthew Yoko, James Massey and N. Swaminathan in the Cambridge University Engineering Department (CUED) are gratefully acknowledged.

A Appendix

The match between RANS and LES using MAP estimate parameters is shown in figs. 10-12 for training cases 1-3 in tab. 1. Corresponding results for testcase 5-6 in tab. 1 are shown in figs. 13 and 14. Note that MAP estimate parameters yield RANS solutions that agree well with the LES in all cases. The increased jet spreading rate is also apparent in the results for $\bar{U}_z$ in figs. 10d-14d. As discussed in the paper, this is due to the absence of additional terms accounting for flow three-dimensionality [20, 22].

REFERENCES

[1] Poinsot, T., and Veynante, D., 2005. Theoretical and numerical combustion. RT Edwards, Inc.

[2] Parente, A., Malik, M. R., Contino, F., Cuoci, A., and Dally, B. B., 2016. "Extension of the eddy dissipation concept for turbulence/chemistry interactions to mild combustion". Fuel, **163**, pp. 98–111.

[3] MacKay, D. J., 2003. Information theory, inference and learning algorithms. Cambridge university press.

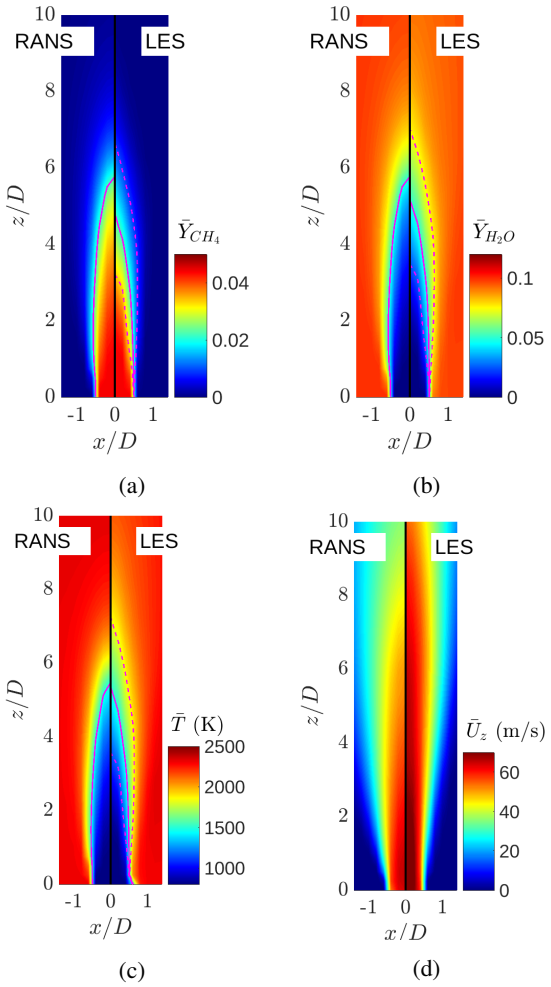

FIGURE 11: Typical comparison between time averaged RANS and LES solutions for LES case 2 ($\phi = 0.8$, $U_c = 68$ m/s) using MAP estimate RANS model parameter values, (a) $\bar{Y}_{CH_4}$ (b) $\bar{Y}_{H_2O}$ (c) $\bar{T}$ (d) $\bar{U}_z$. In each figure, the left half shows the RANS result and the right half the time averaged LES result. The solid magenta curves in (a-c) show mean progress variable $\bar{c} = 0.5$ contours. The broken magenta curves on LES results in (a-c) show $\bar{c} = 0.5$ contours for fields separated by one standard deviation from the mean field. Data is plotted on the comparison mesh.

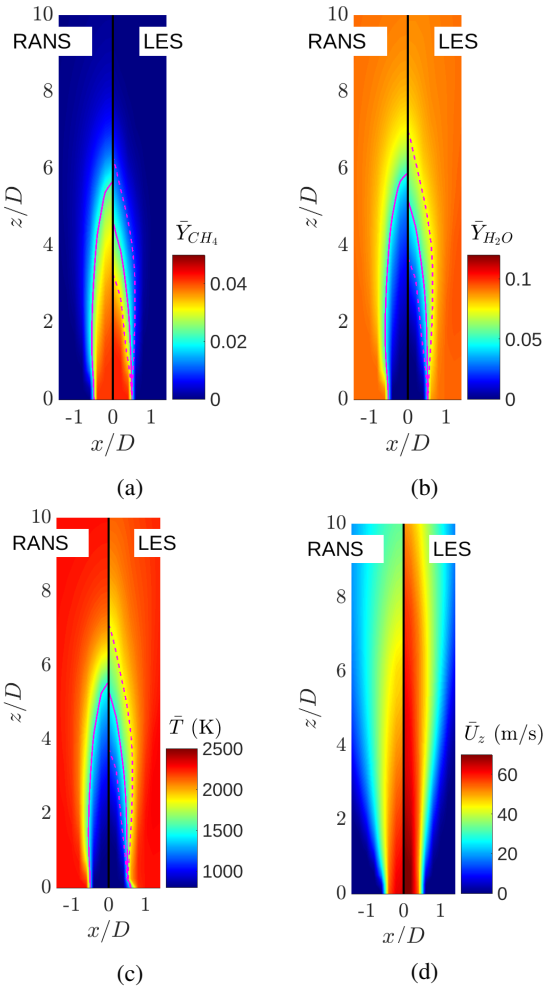

FIGURE 12: Typical comparison between time averaged RANS and LES solutions for LES case 3 ($\phi = 0.76$, $U_c = 64$ m/s) using MAP estimate RANS model parameter values, (a) $\bar{Y}_{CH_4}$ (b) $\bar{Y}_{H_2O}$ (c) $\bar{T}$ (d) $\bar{U}_z$. In each figure, the left half shows the RANS result and the right half the time averaged LES result. The solid magenta curves in (a-c) show mean progress variable $\bar{c} = 0.5$ contours. The broken magenta curves on LES results in (a-c) show $\bar{c} = 0.5$ contours for fields separated by one standard deviation from the mean field. Data is plotted on the comparison mesh.

[4] MacKay, D. J., 1992. "Information-based objective functions for active data selection". Neural computation, **4**(4), pp. 590–604.

[5] Juniper, M. P., and Yoko, M., 2022. "Generating a physics-based quantitatively-accurate model of an electrically-heated rijke tube with bayesian inference". Journal of Sound and Vibration, **535**, p. 117096.

[6] Cheung, S. H., Oliver, T. A., Prudencio, E. E., Prudhomme, S., and Moser, R. D., 2011. "Bayesian uncertainty analysis with applications to turbulence modeling". Reliability Engineering & System Safety, **96**(9), pp. 1137–1149.

[7] Edeling, W. N., Cinnella, P., Dwight, R. P., and Bijl, H., 2014. "Bayesian estimates of parameter variability in the k–ε turbulence model". Journal of Computational Physics, **258**, pp. 73–94.

[8] Xiao, H., and Cinnella, P., 2019. "Quantification of model uncertainty in rans simulations: A review". Progress in Aerospace Sciences, **108**, pp. 1–31.

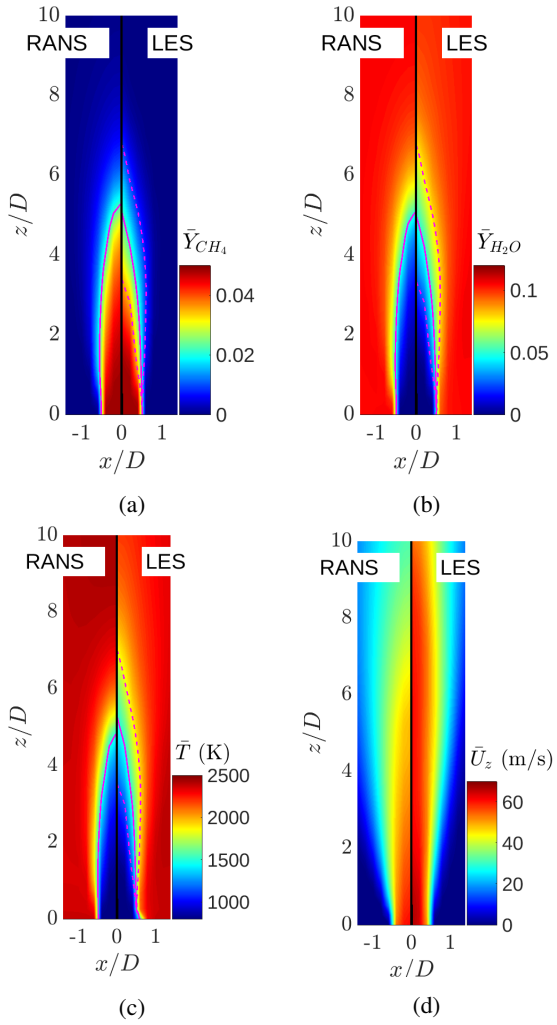

FIGURE 13: Typical comparison between time averaged RANS and LES solutions for LES case 5 ($\phi = 0.88$, $U_c = 60$ m/s) using MAP estimate RANS model parameter values, (a) $\bar{Y}_{CH_4}$ (b) $\bar{Y}_{H_2O}$ (c) $\bar{T}$ (d) $\bar{U}_z$. In each figure, the left half shows the RANS result and the right half the time averaged LES result. The solid magenta curves in (a-c) show mean progress variable $\bar{c} = 0.5$ contours. The broken magenta curves on LES results in (a-c) show $\bar{c} = 0.5$ contours for fields separated by one standard deviation from the mean field. Data is plotted on the comparison mesh.

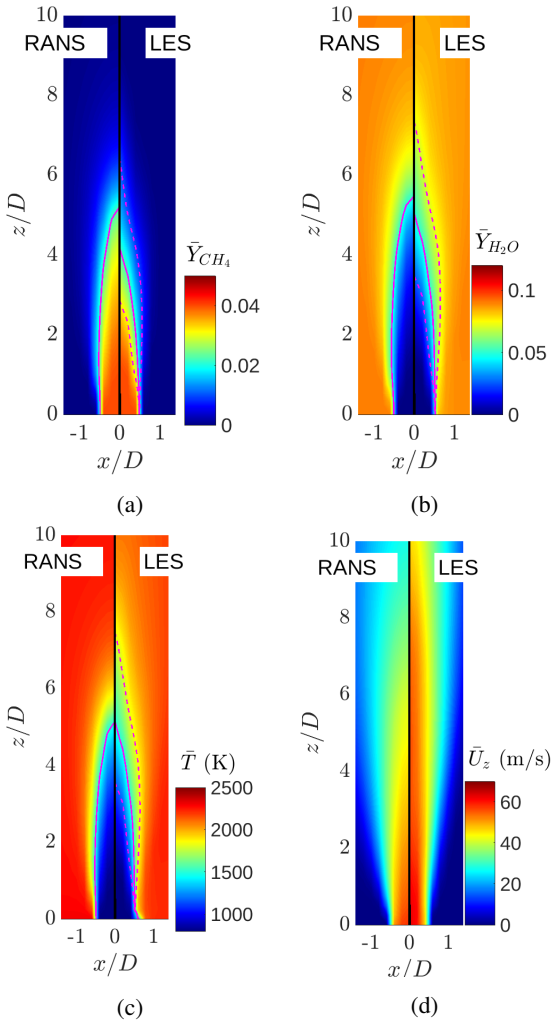

FIGURE 14: Typical comparison between time averaged RANS and LES solutions for LES case 6 ($\phi = 0.72$, $U_c = 56$ m/s) using MAP estimate RANS model parameter values, (a) $\bar{Y}_{CH_4}$ (b) $\bar{Y}_{H_2O}$ (c) $\bar{T}$ (d) $\bar{U}_z$. In each figure, the left half shows the RANS result and the right half the time averaged LES result. The solid magenta curves in (a-c) show mean progress variable $\bar{c} = 0.5$ contours. The broken magenta curves on LES results in (a-c) show $\bar{c} = 0.5$ contours for fields separated by one standard deviation from the mean field. Data is plotted on the comparison mesh.

[9] Datta, A., Mathew, J., and Hemchandra, S., 2022. "The explicit filtering method for large eddy simulations of a turbulent premixed flame". Combustion and Flame, **237**, p. 111862.

[10] Openfoam - opensource cfd software. https://www.openfoam.com/news/main-news/openfoam-v2206.

[11] Pope, S. B., and Pope, S. B., 2000. Turbulent flows. Cambridge university press.

[12] Magnussen, B. F., 2005. "The eddy dissipation concept: A bridge between science and technology". In ECCOMAS thematic conference on computational combustion, Vol. 21, Libson, Portugal, p. 24.

[13] Mathew, J., Lechner, R., Foysi, H., Sesterhenn, J., and Friedrich, R., 2003. "An explicit filtering method for large eddy simulation of compressible flows". Physics of fluids,

15(8), pp. 2279–2289.
[14] Mathew, J., Foysi, H., and Friedrich, R., 2006. "A new approach to les based on explicit filtering". International journal of heat and fluid flow, **27**(4), pp. 594–602.
[15] Sankaran, R., Hawkes, E. R., Chen, J. H., Lu, T., and Law, C. K., 2007. "Structure of a spatially developing turbulent lean methane–air bunsen flame". Proceedings of the combustion institute, **31**(1), pp. 1291–1298.
[16] Visbal, M. R., and Gaitonde, D. V., 2002. "On the use of higher-order finite-difference schemes on curvilinear and deforming meshes". Journal of Computational Physics, **181**(1), pp. 155–185.
[17] Carpenter, M. H., Gottlieb, D., and Abarbanel, S., 1994. "Time-stable boundary conditions for finite-difference schemes solving hyperbolic systems: methodology and application to high-order compact schemes". Journal of Computational Physics, **111**(2), pp. 220–236.
[18] Poinsot, T. J., and Lelef, S., 1992. "Boundary conditions for direct simulations of compressible viscous flows". Journal of computational physics, **101**(1), pp. 104–129.
[19] Bodony, D. J., 2006. "Analysis of sponge zones for computational fluid mechanics". J. Comp. Phys., **212**, pp. 681 – 702.
[20] Pope, S., 1978. "An explanation of the turbulent round-jet/plane-jet anomaly". AIAA journal, **16**(3), pp. 279–281.
[21] Sarkar, S., and Lakshmanan, B., 1991. "Application of a reynolds stress turbulence model to the compressible shear layer". AIAA journal, **29**(5), pp. 743–749.
[22] Thies, A. T., and Tam, C. K., 1996. "Computation of turbulent axisymmetric and nonaxisymmetric jet flows using the k-epsilon model". AIAA journal, **34**(2), pp. 309–316.
[23] Smith, G. P., Golden, D. M., Frenklach, M., Moriarty, N. W., Eiteneer, B., Goldenberg, M., Bowman, C. T., Hanson, R. K., Song, S., William C. Gardiner, J., Lissianski, V. V., and Qin, Z. `http://www.me.berkeley.edu/gri\_mech/`.
[24] Lagarias, J. C., Reeds, J. A., Wright, M. H., and Wright, P. E., 1998. "Convergence properties of the nelder–mead simplex method in low dimensions". SIAM Journal on optimization, **9**(1), pp. 112–147.